EUROPEAN ORGANIZATION FOR NUCLEAR RESEARCH
ORGANISATION EUROPEENNE POUR LA RECHERCHE NUCLEAIRE

CERN - PS DIVISION

PS/DI Note 99-21

VACUUM CHANGES DURING ACCUMULATION OF Pb^{54+} IN LEIR

N. Madsen

Geneva, Switzerland
November 18, 1999

Contents

Chapter I

Introduction

The former Low Energy Antiproton Ring (LEAR) is being converted to a Low Energy Ion Ring (LEIR) for ion accumulation for the LHC [40]. A scheme for accumulation of Lead ions has already been investigated [14], and at present the accumulation time as well as the number of accumulated ions are about a factor of 2 from the design goal.

During these experiments it was observed that the vacuum in the machine increased with the increased beam intensity, this again lead to increased losses - which turned out to be a limitation to the final maximum intensities which could be attained.

In this note we first investigate the various mechanisms responsible for particle losses in LEAR. Among these mechanisms charge-exchange is the most dominant, and using measured values for cross sections for the different reactions we estimate the expected loss rates in LEAR and compare with earlier results on LEAR.

The next step is a study on how the beam and the beam losses affects the vacuum of the machine. Two main mechanism are investigated. One mechanism is due to the beam induced ionization of the residual gas, which is therefore investigated. As the ionized residual gas caused problems in the former ISR, this is investigated in some detail and comparisons are made. Finally we study the effect of direct losses impinging on the vacuum chamber of the machine.

The purpose of these studies is to identify the mechanism responsible for the pressure rise observed in LEAR during accumulation, and suggest possible remedies for this problem.

Chapter II

Particle Losses

A first step in evaluating the mechanisms responsible for the pressure rise and following degradation of the lifetime and therefore the maximum accumulated intensity in the LEAR experiments is to understand which mechanisms governs the particle losses in the experiments.

Therefore, possible mechanisms for beam loss are identified and studied and the influence in the present experiments is evaluated and the mechanisms responsible in the LEAR experiments are identified. This follows to some extent studies which have already been done, but as the information is needed in order to evaluate the influence of vacuum changes on the beam loss the discussion has been included. Some additional information which has not been included in earlier, published, studies is also included.

2.1 Mechanisms for beam deterioration

In the following we list and briefly discuss the known mechanisms which can lead to particle losses from particle beams. Following that we will then discuss the various mechanisms in detail in order that we can evaluate the contribution to the actual beam loss caused by each of them.

1. Electron capture and electron loss processes in interactions with the residual gas may cause charge change of the circulating particles which may again cause these to exceed the acceptance of the machine and therefore be lost. The interaction with the electrons in the electron cooler is also important [14, 62].

2. Multiple Coulomb scattering on the nuclei of the residual gas leads to emittance growth, and will if not countered eventually lead to a beam larger than the machine acceptance and thereby cause losses.

3. Intra beam scattering equilibrates the beams three degrees of freedom, and through the storage ring lattice energy from the total kinetic energy of the beam is coupled into the relative motion in the center-of-mass, which cause emittance growth.

4. Single Coulomb scattering on the nuclei of the residual gas are large angle Coulomb scattering events which, in one event, cause a beam particle to be scattered outside the acceptance of the machine, and thereby lost.

5. Single Coulomb scattering in the beam (Touschek effect) is caused by large angle Coulomb collisions inside the beam. This effect leads to tails in momentum as well as in emittance, these tails may eventually be outside the acceptance of the machine. This effect is most pronounced in electron machines, where the difference between the transverse and the longitudinal temperature may be large [10].

6. Nuclear collisions with the residual gas cause immediate particle loss, but are only important at high energies where the particle may get close enough for the nuclear forces to reach, and where the other effects have become negligible.

7. Instabilities can be caused by mistuning of the ring, which cause the betatron tune to be resonant with the ring periodicity, these lead to particle losses. By careful operation these can usually be avoided.

In the following discussion we will not consider emittance augmenting mechanisms as these will be assumed countered by electron cooling as in the tested scheme for accumulation. However, these may be important as the speed of the cooling is important in order to reach the design accumulation time, which in the experiments so far is about a factor 2 to long [14].

Furthermore nuclear interactions lead to cross sections which are very small at the studied energy of 4.2 MeV/amu, and we will therefore not concern ourselves with nuclear interactions [45]. As instabilities is a phenomenon which is well understood and methods to avoid losses due to these are well known we shall not discuss them here either.

2.2 Scattering of beam particles

We discussed several of these techniques in a recent note [45]. As mentioned in that note and above only single Coulomb scattering is important for losses at relatively low energies in a cooled stored proton beam. In Ref. [45] the loss rate due to single Coulomb scattering of (anti)protons was found. Ignoring the electrons around the nuclei, who contribute an energy loss rather than a scattering [38], we can extend this result to Lead ions with a nuclear charge Z. In doing this we need to take into account that the lead ions are heavier than the residual gas atoms (mass number A). We find a loss rate given by[1]

$$\Gamma = \frac{2\pi Z^2 r_p^2 c n_{sc}}{A^2 \gamma^2 \beta^3} \left(\frac{\beta_h}{\epsilon_{accep,h}} + \frac{\beta_v}{\epsilon_v} \right) \tag{2.1}$$

[1]The calculation in Ref. [45] assumes that the mass of the projectile is larger than the target. This is not the case here, however the scattering angles are still relatively small and the equation can therefore still be used approximatively [60].

where r_p = 1.535·10^{-18} m is the classical proton radius, γ and β are relativistic factors, ϵ_{accep} is the acceptance of the machine, $\beta_{h,v}$ the ring averaged beta functions, c the speed of light and n_{sc} the single Coulomb scattering density given by

$$n_{sc} = \sum {Z_i}^2 n_i \tag{2.2}$$

where n_i and Z_i are the densities and nuclear charge numbers of the residual gas constituents. The vacuum composition and LEAR parameters are given in appendix A. With the standard LEAR vacuum of 5·10^{-12} Torr and various measured compositions given in Table A.2 and Table A.4 the multiple scattering density is in the range 1.6·10^{12} m^{-3} to 1.0·10^{13} m^{-3}. These densities results in loss rates in the range of 10^{-7} s^{-1} to 10^{-6} s^{-1}, which are very small compared to the observed rates in Ref. [14] (0.06 s^{-1} to 0.1 s^{-1}). It must therefore, as mentioned in Ref. [14], be charge-exchange with the residual gas which dominates.

2.3 Charge-exchange processes

Charge-exchange processes consists of electron capture processes and electron loss processes. The equilibrium charge state is the charge state at which the probability for loss and capture are equal. This means that if a particle is passing through a medium it will eventually be in an equilibrium charge state depending on that medium. An approximate formula for the equilibrium charge state for a heavy ion with nuclear charge number Z and velocity β passing through a gaseous medium is given in [26]

$$\bar{q} \approx Z\left(1 - \exp\left(-\frac{\beta}{\alpha_s Z^{0.67}}\right)\right) \tag{2.3}$$

where α_s = 1/137 is the fine structure constant. For Pb ions with a velocity β = 0.094 we find that $\bar{q} \approx 40$. As the charge state of interest for the LEIR is Pb^{54+}, we expect electron capture processes to be the dominant charge-exchange process.

In order to calculate the beam particle loss rate we can use a series of measurements on the electron capture and loss cross sections of 4.66 MeV/amu Pb^{54+} ions done by Graham *et al.* [31]. The measurements are reproduced in Table 2.1.

Adding these cross sections and assuming that any of the reactions will cause loss of the ion, we find that the total loss rate is given by

$$\Gamma_{c-ex} = \beta c \sum n_i \sigma_i \tag{2.4}$$

where σ_i is the cross section for the given species and n_i is its absolute density in the vacuum chamber. If we assume that the vacuum (5·10^{-12} Torr) is only Hydrogen we find a loss rate of 7.4·10^{-4} s^{-1} - much lower than the observed loss rates.

In Ref. [56] is given an empirical scaling law for the cross sections which is based on all the data measured by Graham and others. As our standard vacuum contains both Oxygen and Carbon we need to take these into account, especially as it seems that the loss contribution from collisions with Hydrogen is negligible compared to the observed losses.

Target	$\sigma_{q,q-1}$	$\sigma_{q,q-2}$	$\sigma_{q,q+1}$	$\sigma_{q,q+2}$	σ_{tot}
$(_1H)_2$	0.38	0.021	0.25		0.65
$_2$He	0.89		0.28		1.17
$(_7N)_2$	88	9.0	3.2		100
$_{10}$Ne	48	10.3	1.8	0.23	60.3
$_{18}$Ar	83	21	2.5		106.5
$_{54}$Xe	75	26	3.9		105

Table 2.1: Cross sections for electron capture and electron loss processes for 4.66 MeV/amu Pb^{54+} ions incident on various targets. The typical uncertainty in these values is $\pm 5\%$ [31]. The unit of the cross sections is 10^{-18} cm^2/atom (10^{-18} cm^2/molecule for H_2 and N_2 targets.

The scaling law for single electron-capture is as follows

$$\tilde{\sigma}_{sc} = \frac{1.1 \cdot 10^{-8}}{\tilde{E}^{4.8}} \left[1 - \exp(-0.037\tilde{E}^{2.2})\right] \times \left[1 - \exp(-2.44 \cdot 10^{-5}\tilde{E}^{2.6})\right] \tag{2.5}$$

where the so-called reduced (kinetic) energy $\tilde{E}$ and reduced cross section $\tilde{\sigma}$ are connected to the physical values by

$$\tilde{\sigma}_{sc} = \sigma_{sc}\frac{Z_t^{1.8}}{q^{0.5}} \;\; ; \;\; \tilde{E} = \frac{E}{Z_t^{1.25}q^{0.7}} \text{ [keV/amu]} \tag{2.6}$$

One interesting facet of this empirical scaling law is that is it valid for a rather large energy range E_k (0.3 to 8.5 MeV/amu) as well as a large range of charge states q (3+ to 59+). Furthermore it is independent of the chemical nature of the projectile, i.e. it depends only on its charge state. Figure 2.1 shows a comparison of data for Pb^{54+} ions and this scaling law. In the figure is also shown results from Franzke's formula [25], which has been used in earlier studies [40]. Franzke introduces two formulas one for electron capture and one for electron loss, these are given as

$$\sigma_C = 2.0 \cdot 10^{-24}\frac{\bar{q}^2\bar{q_T}}{Z^{0.5}(\gamma^2-1)^2}\left(\frac{q}{\bar{q}}\right)^2 \text{cm}^2\text{/atom} \; ; \; Z \geq 36 \; ; \; \gamma < 1.1 \tag{2.7}$$

$$\sigma_L = 3.0 \cdot 10^{-18+(0.71\log Z)^{3/2}}\frac{\bar{q_T}}{\bar{q}^2\sqrt{\gamma^2-1}}\left(\frac{q}{\bar{q}}\right)^{-4} \text{cm}^2\text{/atom} \; ; \; Z \geq 36; \gamma < 1.1 \tag{2.8}$$

for high charge states $q > \bar{q}$. The parameters $\bar{q}$ and $\bar{q_T}$ are the equilibrium charge states for projectiles of velocity β of the projectile and target respectively given by equation (2.3).

It should be noted that Franzke's formula is supposed to calculate the total electron capture (loss) cross section. Schlachter's scaling rule for electron capture is for single electron capture. The contribution from higher order interactions is usually less than 20%, however as none of the two equations predict the cross sections with a precision of this order Schlachter's formula has been chosen for this work as it seems to follow the cross section variation with target better than Franzke's, especially for the lighter targets which are abundant in vacuum systems.

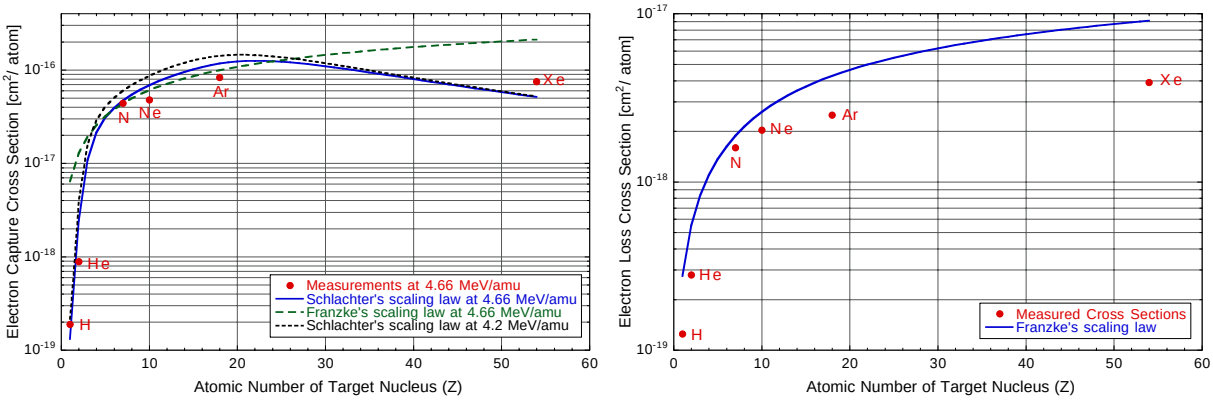

Figure 2.1: Left: Single electron capture cross sections for Pb^{54+} ions. The points are experimental results [31], the solid line an empirical scaling law from Ref. [56] and the long dashed line is Franzke's formula eqn. (2.7). Right: Electron loss cross sections for Pb^{54+} ions at 4.66 MeV/amu. The solid line is Franzke's loss formula eqn. (2.8).

The right plot in Figure 2.1 shows the cross sections for single electron loss, together with equation (2.8). It is interesting to note that the energy dependence seems to be wrong in eqn. (2.8), a conclusion which we deduce from the fact that the equation was originally fitted to experimental data taken at an energy of 1.4 MeV/amu [25]. However, from the experiments discussed in Ref. [57] we find that the loss cross section does not depend strongly on energy in the energy regime 3 - 9 MeV/amu - thus the loss cross sections measured at 4.66 MeV/amu can be used at 4.2 MeV/amu. No cross sections for electron loss in Oxygen or Carbon has been found in the literature, but from Figure 2.1 we conclude that we can approximate the scaling around these Z values to be linear in Z, thus we estimate the cross sections for Oxygen and Carbon atoms by calculating $Z_{O,C}/Z_N \cdot \sigma_{loss}(N)$ (the precision is anyway not much better than 20% thus there is no point in going into more detail).

In Table A.7 in the appendix we have calculated the loss rates for 8 different vacuum compositions with the same absolute pressure of $5{\cdot}10^{-12}$ Torr. These calculations results in loss rates in the range $5.5{\cdot}10^{-3}$ s^{-1} to $3.6{\cdot}10^{-2}$ s^{-1}. The measured loss rates given in Ref. [14] vary between $5{\cdot}10^{-2}$ s^{-1} and $1{\cdot}10^{-1}$ s^{-1}. As the pressure in LEAR at times could easily be 10^{-11} Torr, there seems to be a reasonable agreement between the observed and the calculated loss rates.

A loss rate of $5{\cdot}10^{-2}$ s^{-1} corresponds to $5{\cdot}10^{6}$ ions being lost per second for a beam of 10^{8} particles, and thus impinging on the chamber walls with more or less their full energy of 4.2 MeV/amu. Furthermore the injection efficiency was about 50%, thus with a continuous supply of 10^{8} ions every 0.4 s, about $1{\cdot}10^{8}$ are lost on the chamber walls per second (i.e. the losses due to the beam lifetime are negligible in this context).

2.4 Loss dynamics

In the previous sections we have argued that most losses occur due to charge-exchange processes, and that the dominant part of these are electron capture processes.

It is interesting to consider what happens after a charge-changing collision as the loss mechanism and hence the angle of impact of the lost particle on the vacuum chamber may be important for the influence of the loss on the vacuum of the machine.

Particles in a storage ring like LEAR are confined by magnetic forces, thus the influence of a charge change can be understood by a glance at the Lorentz force [38]

$$\mathbf{F} = q\left(\mathbf{E} + \frac{\mathbf{v}}{c}\times\mathbf{B}\right) \tag{2.9}$$

where $\mathbf{E}$ is the electrical field, which is zero in our case, $\mathbf{v}$ the velocity of the particle, c the speed of light and $\mathbf{B}$ the magnetic field.

From the Lorentz force we see that a change in the charge has the same influence as a change in the velocity. The lead ions in question here are non-relativistic, thus a change in velocity corresponds to a change in momentum, and a change in momentum leads to a change of the equilibrium orbit. The equilibrium orbit of a particle with a momentum deviation compared to the ideal particle is the dispersion orbit, which to first order is given by

$$x(s) = D(s)\frac{\Delta p}{p} \tag{2.10}$$

where $D(s)$ is the dispersion function and $x(s)$ is the local deviation of the orbit. Due to the Lorenz force we may consider a charge change the same way we consider a momentum change, thus all the limitations and rules regarding $\Delta p/p$ are equivalent for $\Delta q/q$. This means that the longitudinal acceptance of the machine can be used. The longitudinal acceptance given in Table A.1 is $\pm$ 4·10^{-3}. As a change of the ion charge by one corresponds to $\Delta q/q$ = 2·10^{-2} is it clear that the particles are lost with just one charge change. Until the loss they will follow the dispersion orbit, and they will thus be scraped at some acceptance limiting point. This simple consideration is in agreement with the variation of the pressure rise around the ring observed in Ref. [14]. Thus it depends on the nature of the acceptance limitations whether the particle will be lost with a large or small angle of incidence on the chamber walls, a fact which may be important as the interaction of a particle with a surface may depend strongly on its angle of incidence [41, 59].

2.5 Summary

We have looked at a few mechanisms causing beam loss in the machine in order to establish which changes are needed in order to increase the loss rate as observed in LEAR. We observe that non-Hydrogen components in the vacuum severely affects the lifetime of the beam and should therefore be kept to a minimum. The large influence of non-Hydrogen constituents in the vacuum manifests itself due to a scaling with $\approx Z_t^{2.5}$ for $Z_t < 10$.

Most of the lost Pb ions will impinge on the vacuum chamber walls with essentially the nominal energy and it is therefore interesting to study their desorption yield compared to the influence of the ionized rest-gas ions. It is worth noting that the bulk of the directly lost particles actually stems from a bad injection efficiency, thus if these turn out to be responsible for the pressure rise, a lot may be gained from improving the injection efficiency.

Chapter III

Beam induced vacuum changes

As we saw in the previous section the residual gas has a large impact on the beam lifetime and quality. However, the opposite is also the case, that is that the passage of the beam through the residual gas influence the residual gas. Significant influence has been observed at several machines around the world. The observed effects can be summarized as follows

1. The passage of the beam ionizes the residual gas. If the beam is positive (protons, most ions) the ions created will be accelerated away from the beam and onto the vacuum chamber, where they may cause desorption of adsorbed gas molecules[1].

2. Collisions of lost particles with the vacuum chamber walls may induce desorption of adsorbed gas molecules directly.

3.1 Ionization of the residual gas

Ionization of the residual gas, is a problem which has already been studied intensively in high energy machines such as the ISR [32], where instabilities due to acceleration of beam induced rest-gas ions in the space-charge field from the beam arose. This has also been studied intensively for the future LHC [18].

The rate of ionization of the residual gas is therefore important. As the problems encountered in the experiments described in Ref. [14] never were observed with antiproton or proton storage in LEAR one may suspect that the ionization rate and the following desorption could be increased by the change to a Pb^{54+} beam.

The cross section for ionization by fast singly charged particles can be described by the Bethe formula [30], which is given by

$$\sigma_{Bethe} = 4\pi a_0^2 \frac{\alpha^2}{\beta^2} \times \left\{ M_{ion}^2 \left[\ln\left(\frac{\beta^2}{1-\beta^2} \right) - \beta^2 \right] + C_{ion} + \gamma_{ion} \frac{\alpha^2}{\beta^2} \right\} \tag{3.1}$$

[1] In the case of negative beam particles (antiprotons or electrons) the ionized residual gas atoms will be trapped by the beam potential and possibly induce instabilities.

where α is the fine structure constant, a_0 is the Bohr radius, βc is the projectile velocity, and M_{ion}, C_{ion} and γ_{ion} are target specific parameters which have been found empirically [52, 30]. Note that the Bethe formula is independent of the projectile mass and the sign of the projectile charge. At low energy (below about 2 MeV/amu [4]) the sign becomes important, as the interaction is no longer a simple Coulomb collision between the target electrons and the projectile, but rather a collision with the atom as a whole[2].

For particles with charges q larger than one, the ionization cross section has been found to scale as [30]

$$\sigma_i = q^2 \exp\left[-\lambda(q^{1/2}\alpha/\beta)^2\right] \sigma_{Bethe} \tag{3.2}$$

where λ is an target specific parameter which can be determined empirically.

In Table 3.1 the target specific parameters are listed for a selection of typical rest gas components, and some rare gases.

Species	Mass	Z	M_{ion}^2	C_{ion}	γ_{ion}	λ
H_2	2	2	0.7	8.12	-1.3	1.0
He	4	2	0.75	7.7	-1.21	2.0
CH_4	16	10	4.2	41.85		
H_2O	18	10	3.24	32.36		
N_2	28	14	3.74	34.84		
CO	28	14	3.7	35.14		
O_2	32	16	4.2	38.84		
Ar	40	18	4.22	37.93		
CO_2	44	22	5.75	56		
Xe	131	54	8.04	72.35		

Table 3.1: Ionization parameters for a range of molecules and atoms [52, 30].

With the values in Table 3.1 is is possible to calculate the ionization cross sections for Pb^{54+} ions at 4.2 MeV/amu. It should however be noted that neither the γ_{ion} nor the λ values have been measured for species other than where listed. As the γ_{ion} is a low energy correction factor, irrelevant at 4.2 MeV/amu we choose to set this equal to zero for the unknown values. However the λ which is also a low energy correction has some influence for Pb^{54+} ions at 4.2 MeV/amu which is the reason why we have included the Xe atom in the list above, as this is one of the few species for which the ionization cross section has been measured with lead ion impact at 4.2 MeV/amu, and we will use this and a few other measurements to extrapolate the λ values for the unmeasured species. Table 3.2 shows the few available measured ionization cross sections.

With these cross section in hand, we have chosen the λ values listed in Table 3.3, and find the cross sections also listed in that table.

[2]This issue is also addressed in Ref. [51], however the low energy deviation is not mentioned, and one might be confused by a statement saying that the cross section is independent of the projectile charge - which is clearly wrong.

Target	Pb Energy	σ_+	Ref.
$({}_1H)_2$	4.65 MeV/amu	$220^{+24}_{-30}\cdot 10^{-16}$ cm^2	[54]
${}_{18}$Ar	4.65 MeV/amu	$640^{+70}_{-100}\cdot 10^{-16}$ cm^2	[53]
${}_{54}$Xe	4.65 MeV/amu	$1560^{+190}_{-250}\cdot 10^{-16}$ cm^2	[53]

Table 3.2: Ionization cross sections for various typical residual gas constituents being ionized by a passing Pb^{54+} beam. One observation made in the various studies quoted is that the cross section does not depend on the chemical species of the incident particle, but only on its E_k/amu and its charge state q.

Species	Mass [amu]	Z	λ	σ_i(4.65) [10^{-16} cm^2]	σ_{exp}(4.65) [10^{-16} cm^2]	σ_i(4.2)
H_2	2	2	1.0	203	220^{+24}_{-30}	214
He	4	2	2.0	131		134
CH_4	16	10	1.5	804		833
H_2O	18	10	1.5	623		645
N_2	28	14	1.5	629		650
CO	28	14	1.5	646		668
O_2	32	16	1.5	696		719
Ar	40	18	1.6	641	640^{+70}_{-100}	659
CO_2	44	22	1.5	1054		1091
Xe	131	54	0.8	1547	1560^{+190}_{-250}	1631

Table 3.3: Comparison of calculated and measured ionization cross sections for Pb^{54+} impact at 4.65 MeV/amu and the calculated ionization cross sections at 4.2 MeV/amu.

It is worth noting that these ionization cross sections are considerably higher (mainly due to the q^2 scaling in equation (3.2), see Figure 3.1)) than the ones for typical residual gas species for protons at the ISR energies, as well as for protons at 4.2 MeV/amu [52]. Using the results in Ref. [52] we find ionization cross sections for typical residual gases for protons of 4.2 MeV/amu of order 10^{-17} cm^2 and at the ISR the energy of 26 GeV of order 10^{-18} cm^2, both several orders of magnitude smaller than for lead ions at 4.2 MeV/amu.

Another interesting aspect of ionization cross sections is that for highly charged projectiles such at Pb^{54+} the relative probability for multiple ionization (loss of more electrons of the target) is enhanced [53, 48, 9]. Thus we would expect that only about half the total cross section is single ionization and the rest is double or higher[3] (depending naturally of whether that is possible in the target).

From the ionization cross sections the number of ions generated per unit time of each rest gas

[3] As the charge of the projectile gets large the ratio between multiple ionization and single ionization levels out, thus the largest change in the relation between the cross sections is for low charge states, i.e. the change from protons to Pb^{54+} is large but the change from Pb^{28+} to Pb^{54+} is small [7].

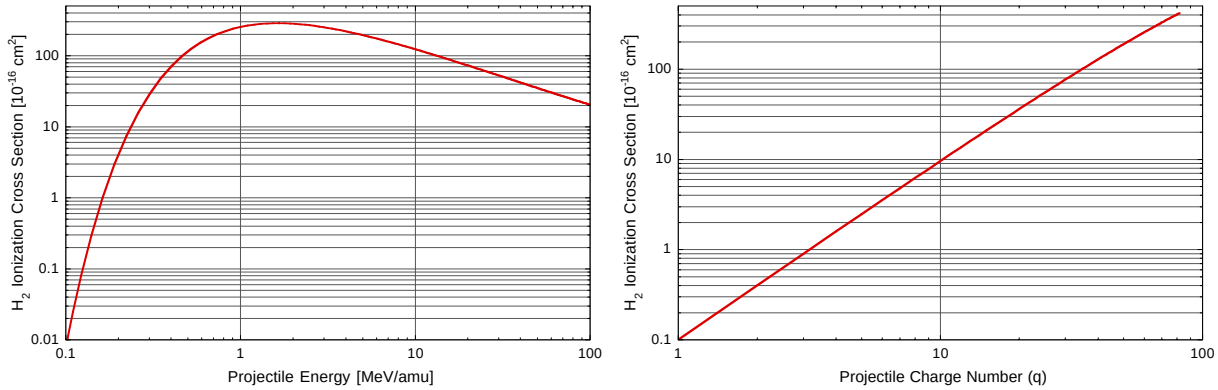

Figure 3.1: Ionization cross sections for a charged particle incident on H_2 gas as a function of energy and charge of the incident ion calculated using eqn. (3.2). The charge state is q=54 in the left plot and the energy is 4.2 MeV/amu in the right plot.

species i can be calculated by(assuming that the generation of ions does not influence the density of neutrals significantly)

$$\frac{dN_{+,i}}{dt} = N\beta c n_i \sigma_{+,i} \tag{3.3}$$

which with some selected vacuum conditions from Appendix A gives the generation rates shown Table 3.4.

Species	Vacuum Composition			
	a	d	e	h
H_2	$1.0{\cdot}10^{7}$	$2.8{\cdot}10^{6}$	$8.6{\cdot}10^{6}$	$6.5{\cdot}10^{6}$
He	0	0	0	0
CH_4	$6.4{\cdot}10^{6}$	$1.3{\cdot}10^{7}$	$1.0{\cdot}10^{7}$	$1.9{\cdot}10^{7}$
H_2O	$1.9{\cdot}10^{5}$	$3.7{\cdot}10^{5}$	$1.8{\cdot}10^{5}$	$1.1{\cdot}10^{6}$
N_2	$5.7{\cdot}10^{5}$	$9.6{\cdot}10^{6}$	0	$1.5{\cdot}10^{5}$
CO	$4.9{\cdot}10^{5}$	$8.3{\cdot}10^{6}$	$3.1{\cdot}10^{6}$	$1.2{\cdot}10^{6}$
O_2	0	$8.1{\cdot}10^{5}$	0	0
Ar	0	$3.7{\cdot}10^{5}$	0	0
CO_2	0	0	$4.3{\cdot}10^{5}$	$5.1{\cdot}10^{5}$
Total	$1.8{\cdot}10^{7}$	$3.5{\cdot}10^{7}$	$2.2{\cdot}10^{7}$	$2.9{\cdot}10^{7}$

Table 3.4: Ions generated per unit time and unit distance (m^{-1} s^{-1}) for various vacuum compositions assuming an absolute pressure of $5{\cdot}10^{-12}$ Torr ($7{\cdot}10^{-10}$ Pa), and a circulating $Pb54+$ beam of 10^8 particles.

Table 3.4 shows an ion production rate of about $3{\cdot}10^{7}$ $m^{-1}s^{-1}$ which should be compared to the linear density of residual gas of about $5{\cdot}10^{9}$ m^{-1}, thus the assumption that only a small fraction is ionized holds reasonably. For comparison the generation of Hydrogen ions in the

ISR at 5A (where the problems emerged initially [33]) with a hydrogen density of 10^{12} cm^{-3} (corresponding to a pressure of $3{\cdot}10^{-13}$ Pa), and a cross section for ionization of $0.22{\cdot}10^{-18}$ cm^{-2} [52], is $7{\cdot}10^{8}$ m^{-1}s^{-1}, an order of magnitude larger. However at the nominal intensity of 10^{9} Pb ions in LEAR the ion production rate would be the same as it was in the ISR per unit length. Thus we need to investigate the ionized residual gas atoms and molecules ability to desorb molecules from the surface of the vacuum chamber.

3.2 Desorption of molecules and atoms from a surface

The interaction of charged particles with a solid can, be split up into two regimes based on the energy or rather the velocity of the projectile. The 'critical' velocity which separates to two regimes is the typical velocity of an electron in an atom called the Bohr velocity $v_b = e^2/4\pi\epsilon_0\hbar \approx 2{\cdot}10^6$ m/s (25 keV/amu). When considering particles moving much slower than this velocity the interaction of the projectile is with the whole atom, whereas when much faster, the projectile "sees the electrons at rest" and electronic collisions occur [11].

This observation is important in trying to understand the desorption mechanisms important for the vacuum in the presence of a circulating beam, as this means that we have (at least) two different subjects to consider. As mentioned earlier the circulating beam ionizes the residual gas, and the space charge potential may accelerate the newly created ions onto the surface of the vacuum chamber where they may desorb adsorbed molecules/atoms. Molecules/atoms can either be physisorbed or chemisorbed on the surface of the material, the corresponding binding energies are typically below 0.3 eV and above 1 eV respectively [58] (see also Appendix B.2).

The accelerating space-charge potentials in question are usually below a couple of kV and the mechanisms responsible for desorption are therefore dominated by interactions with the full atoms. On the other hand we have the direct losses of beam particles due to charge-exchange or single Coulomb scattering which cause particles of high energy to impact on the vacuum chamber surfaces. Furthermore will the ions of the ionized residual gas generally have low charge states (single ionization being the most probable) whereas the fast ions will have high charge states in our specific situation in LEAR.

Because of the possible large difference between the desorption mechanisms, and therefore in the cross sections and scaling laws, we split the discussion in two, starting with the slow ions of the residual gas.

3.2.1 Rest-Gas Ion induced desorption

In the proposed LEIR scheme the number of particles in the beam will vary from $5{\cdot}10^{7}$ at the start of injection to $1.2{\cdot}10^{9}$ before ejection for acceleration to the LHC [14]. The influence of ionization of the rest gas increases with the number of accumulated particles for two reasons. First of all the number of ionizations increase, and secondly the accelerating space-charge potential increases. The space charge field from an axisymmetric Gaussian beam of constant $\sigma_\perp$ is

purely transverse and given by [44]

$$E_{\perp}(r) = \frac{ze\lambda}{2\pi\epsilon_0 r\sigma_{\perp}^2\gamma^2}\left[1 - \exp\left(-\frac{r^2}{2\sigma_{\perp}^2}\right)\right] \tag{3.4}$$

where $\lambda = N/C$ is the linear density in the beam, r is the distance from the center and γ the relativistic factor.

From the space-charge field we can find the potential Φ to be

$$\Phi_{sc}(r) = -\int E_{\perp}(r)dr \tag{3.5}$$

which with the range of intensities foreseen in LEIR gives maximum accelerating potentials of about 12V (it depends on the vacuum chamber radius), significantly lower than the potentials of about 2kV experienced in the ISR [22].

Desorption by ions in this energy range has been investigated intensively, as it has been important both in vacuum systems such as the ISR [16] and LHC [5], but also because bombardment of surfaces with ions cleans the surface, a process called sputtering. It has been found that the desorption yield increases with mass of the bombarding particle [5]. Measurements of the desorption yield as a function of energy reveals that for low energies the yield saturates around 3keV [47], and there is a minimum energy for desorption of a few eV (related to the binding energy of the adsorbates). With suitable cleaning techniques (argon glow discharge) a negative desorption yield was accomplished in the ISR, effectively making the whole of the vacuum chamber into a pump [16].

As the residual gas ions created in LEAR are at very low energy of about 10 eV, the desorption coefficient is extremely low. Using the ISR data for a clean and baked but not glow discharge cleaned vacuum chamber we estimate the desorption yield (conservatively) to be about 0.05 molecules/ion [33]. Thus even if all the ionized rest-gas ions ($3{\cdot}10^7$ $s^{-1}m^{-1}$) reach the vacuum chamber surface and cause desorption, we will have a desorption yield of $1.5{\cdot}10^6$ molecules/m/s, which corresponds to an outgassing rate of $1{\cdot}10^{-14}$ Pa·m/s assuming and average vacuum chamber radius of 0.1 m. Typical outgassing rates for cleaned and well baked stainless steel surfaces are of the order of 10^{-8} Pa·m/s, and some of the best measured outgassing rates of specially coated and treated surfaces are 10^{-12} Pa·m/s [36], thus residual gas ion induced desorption is not a problem for lead ion accumulation in LEAR.

3.3 Direct losses

Apart from desorption due to low energy ions as discussed above, we may also have desorption due to incident lead ions which are outside the acceptance of the machine. This happens both continuously during storage and accumulation as lead ions undergo charge-exchange, but also due to mismatch and over full buckets during injection. In the ISR the desorption due to lost protons was negligible [16].

In LEAR this may be very different as many interaction cross sections, such as for example ionization scales strongly with the charge of the incident projectile. One example is the desorption of H^+ ions from a surface during heavy ion bombardment, which scales with the charge state of the incoming projectile as q^3 [59].

Going through the literature we find that hardly any research has been directed against desorption of 'surface impurities', as we choose to call the adsorbed residual gas molecules, due to highly charged fast heavy ions. The reason seems to be that the main lines of study are interested in cleaning surfaces, and the highest yields are close to the Bohr velocity [20], or into studying fission fragments in reactors impinging on container walls [19, 12]. However the trend in these experiments and theory is that the yield has a maximum around the Bohr velocity but drops only slowly as going to higher velocities, while it increases strongly with the incident charge state, and only depends slightly if not at all on the mass of the projectile [59]. On the other hand most of these studies are concerned with ion desorption, and these in general positive. As the beam itself is positive, it is therefore not obvious whether this is the source of the vacuum increase. However the process of desorption is further complicated by the release of large showers of secondary electrons when the projectile penetrates the material [19, 28]. It would therefore be desirable with measurements of the cross section of desorption of various typical residual gas components due to fast lead ion impact, like what has been measured for low energy singly charged ions impacting on cold surfaces [5].

Recently however, some experimental results from the Brookhaven AGS Booster indicates problems similar to the ones in LEAR [63, 64]. In these experiments it has been observed that beam loss during injection cause increase of the pressure in the machine, which in turn reduces the lifetime. Their beam is an Au^{31+} beam with β = 0.044 (0.9 MeV/amu). They find, similarly to the observations in LEAR that the pressure increase decreases rapidly when the beam is switched off (τ = 35 ms). They have also investigated the pressure dependence on the losses, and they find good agreement between the observed lifetime and the observed increase in pressure.

However, their observations only confirm our suspicions that the problems are caused by direct losses of lead ions, no solution is offered. We can however try to estimate the beam induced increase in outgassing responsible for the pressure increase.

The equilibrium density in a vacuum chamber is proportional to the desorption rate, thus if we assume that the typical desorption in LEAR was $5{\cdot}10^{-9}$ Pa·m/s (= $5{\cdot}10^{-12}$ mbar·l/s/cm^2), a pressure increase of a factor approximately 5 corresponds to a desorption increase by a factor 5. This equals a beam induced desorption of $4{\cdot}10^{-8}$ Pa·m/s = $3{\cdot}10^{1}2$ molecules/m/s. During continuous injection we are loosing approximately 10^8 lead ions onto the chamber walls per second ($1.3{\cdot}10^6$ s^{-1} m^{-1}), thus each ion, if this is the cause, induces the release of $2.5{\cdot}10^6$ adsorbed molecules. For comparison the AGS people estimate 10^5 molecules per lost ion, thus it does not sound unreasonable.

3.4 Conclusions

We have discussed various mechanisms via which a circulating beam may cause changes in the vacuum. One mechanism which was observed to cause problems in the former ISR was

that, the by the beam ionized residual gas atoms/molecules, are accelerated by the space-charge potential of the beam onto the chamber walls of the vacuum system and cause desorption of adsorbed molecules/atoms. In the ISR this lead to a limitation in the maximum circulating current. However though a series of calculations based on cross section for ionization and typical beam parameters in the LEAR experiments we find that the desorption possible via this mechanism in LEAR is negligible compared to the normal outgassing rate of the chamber walls.

However, using the beam loss measurements from LEAR we find that a considerable amount of beam particles are continuously being lost onto the chamber walls. At these energies the knowledge of desorption yields is very limited, and we can therefore not directly conclude that the lost particles are the reason for the pressure increase. However, the interaction of projectiles with targets such as adsorbates has been seen throughout the literature to scale strongly with the charge state of the projectile. Furthermore the at an energy of 4.2 MeV/amu ionization cross sections as well as other cross sections are quite large compared to f.ex. at 26 GeV as in ISR. Thus it seems plausible that the directly lost beam constituents are responsible for the pressure rise. Finally similar observations have been done at the AGS in Brookhaven, and similar conclusions, though no solutions have been drawn [63, 64].

Chapter IV

Conclusions

In light of the pressure rise observed at LEAR during testing of a new scheme for accumulation of lead ions for the LHC experiment ALICE [3], and the limiting influence of this pressure rise on the efficiency of the scheme in terms of the maximum accumulated beam current, we have investigated the interaction of the lead beam with the LEAR vacuum and surroundings in order to establish the source of the unwanted pressure rise.

We have found that the pressure rise is most likely caused by the direct losses of lead ions onto the vacuum chamber walls. Lead ions are lost due to charge-exchange processes with the residual gas, mainly electron capture, but also, and in considerably larger numbers, during injection due to an injection efficiency of only 50%. The lost particles may thus impinge on the chamber walls with their full energy of 4.2 MeV/amu. The high charge state of the lead ions are believed to enhance their ability to desorb material from the chamber walls considerably and thus cause strongly increased desorption and thereby pressure.

Unfortunately no experimental or theoretical information can be found on exactly this process thus it is hard to evaluate what measures should be initiated in order to resolve the issue. However there is no doubt that cleaning the vacuum chamber walls efficiently will help, but without absolute information on desorption yields it is difficult to estimate the level of cleanliness necessary for the pressure rise to be avoided. Naturally a significant increase of the injection efficiency may also help.

A possible remedy of this lack of information is to carry out a series of measurements on the desorption yield due to lead ion impacts. Desorption yields can be measured with a variety of methods [6, 21, 35, 5], and a more detailed study will be needed to find the right setup, something beyond the scope of this note. These measurements should be done for various cleaning methods, and various levels of cleanliness of the subject in order to be able to estimate the necessary level [1, 2, 8, 46]. Furthermore, it would be necessary to investigate the dependence on the incident angle of the projectiles, as large incident angles where the projectile travels along the surface for some time may enhance the desorption yield considerably [59]. Other possibilities, if it turns out that ordinary stainless steel will not be feasible for the vacuum chamber, may consist of studying various surface coatings which have shown desirable behaviour in other ways [17, 29, 37, 49].

Appendix A

Vacuum and LEAR parameters

For the calculations of the losses due to the residual gas a vacuum description (composition and pressure) as well as some ring parameters are needed.

A.1 Accelerator and beam parameters

Table A.1 shows some relevant parameters for LEAR used in the calculations, whose results are given in chapter 2.

Parameter	Symbol	Value
Circumference	C	78.54 m
Bending Radius	ρ	4.2 m
Average Horizontal Beta function	$\langle\beta_h\rangle$	7.2 m
Average Vertical Beta function	$\langle\beta_v\rangle$	8.2 m
Horizontal Acceptance	$\epsilon_{accep,h}$	150 π mm mrad
Vertical Acceptance	$\epsilon_{accep,v}$	40 π mm mrad
Momentum Acceptance	$\Delta p_{accep}/p$	$\pm$ 4·10^{-3}
Average vacuum chamber radius	b	0.1 m
Ion Mass Number	A	208
Nuclear charge number	Z	82
Ion Charge	z	+54
Ion Kinetic Energy	E_{kin}	4.2 MeV/amu
Ion Momentum	p	88.9 Mev/c/amu
Ion Relative Velocity	β	0.094
Number of ions pr. injection	N_{inj}	5·10^7
Design Accumulation Goal	N_0	1.2·10^9

Table A.1: LEAR and Pb beam parameters for the calculations [14, 39].

A.2 LEAR Vacuum

Table A.2 shows the composition of the LEAR vacuum as it was in 1997 during the experiments described in [14]. In Table A.3 the equivalent atomic densities are calculated (assuming room temperature of 300 K), and the relative amount of each species is listed.

	Single Injection		Multiple Injection	
Species	Sect. 2	Sect. 4	Sect. 2	Sect. 4
	[10^{-12} Torr]	[10^{-12} Torr]	[10^{-12} Torr]	[10^{-12} Torr]
H_2	1.30	35.00	1.30	63.00
He	0.00	0.00	0.00	0.00
CH_4	1.00	11.00	0.99	19.00
H_2O	0.07	0.31	0.02	0.44
N_2	0.01	0.00	0.01	0.00
CO	0.08	0.10	0.13	7.30
O_2	0.00	0.00	0.00	0.00
Ar_2	0.00	0.00	0.00	0.00
CO_2	0.02	0.15	0.02	0.62
Total	2.48	46.56	2.47	90.36

Table A.2: LEAR vacuum partial and total pressures (absolute) in two ring sections during multiple injection (accumulation) and during single injection (November 1997).

In studying the composition and pressures one notes that section 4 is generally much worse of than section 2. This is a general tendency for most of the LEAR vacuum measurements.

	Single Injection		Multiple Injection	
Species	Sect. 2	Sect. 4	Sect. 2	Sect. 4
	[m^{-3}]	[m^{-3}]	[m^{-3}]	[m^{-3}]
H	(84%) $2.2{\cdot}10^{11}$	(90%) $3.7{\cdot}10^{12}$	(83%) $2.1{\cdot}10^{11}$	(85%) $6.5{\cdot}10^{12}$
C	(14%) $3.5{\cdot}10^{10}$	(9%) $3.6{\cdot}10^{11}$	(14%) $3.7{\cdot}10^{10}$	(11%) $8.7{\cdot}10^{11}$
N	(0%) $6.4{\cdot}10^{8}$	(0%) $0.0{\cdot}10^{0}$	(0%) $6.4{\cdot}10^{8}$	(0%) $0.0{\cdot}10^{0}$
O	(2%) $6.1{\cdot}10^{9}$	(1%) $2.3{\cdot}10^{10}$	(2%) $6.1{\cdot}10^{9}$	(4%) $2.9{\cdot}10^{11}$

Table A.3: LEAR vacuum atomic densities in two ring sections during multiple injection (accumulation) and during single injection.

From Table A.3 we see that in section 2 the influence of the multiple injection is negligible, whereas in section 4 the presure doubles and the relative abundance of Hydrogen decreases.

In order not to draw wrong conclusions Table A.4 lists another measurement (September 1997) of the pressure and rest gas composition in LEAR.

In the September measurements in Table A.4 we once again observe that section 4 is bad compared to 2 and as it turns out compared to all other sections. Table A.5 on the other hand

Species	Sect. 1 [10^{-12} Torr]	Sect. 2 [10^{-12} Torr]	Sect. 3 [10^{-12} Torr]	Sect. 4 [10^{-12} Torr]
H_2	0.23	1.6	0.49	33.0
He	0.00	1.9	0.14	0.0
CH_4	0.27	1.0	2.7	5.3
H_2O	0.01	0.04	0.06	0.2
N_2	0.26	0.20	0.12	0.6
CO	0.22	0.17	0.10	0.5
O_2	0.02	0.02	0.00	0.0
Ar_2	0.01	0.8	0.01	0.0
CO_2	0.00	0.03	0.02	0.0
Total	1.0	5.7	3.6	39.6

Table A.4: LEAR vacuum partial and total pressures (absolute) in the four different ring sections (September 1997).

Species	Sect. 1 [m^{-3}]	Sect. 2 [m^{-3}]	Sect. 3 [m^{-3}]	Sect. 4 [m^{-3}]	Variation [n_{max}/n_{min}]
H	(55%) $5.0{\cdot}10^{10}$	(61%) $2.3{\cdot}10^{11}$	(78%) $3.8{\cdot}10^{11}$	(92%) $2.8{\cdot}10^{12}$	56
He	(0%) $0.0{\cdot}10^{0}$	(16%) $6.1{\cdot}10^{10}$	(1%) $4.5{\cdot}10^{9}$	(0%) $0.0{\cdot}10^{0}$	-
C	(17%) $1.6{\cdot}10^{10}$	(10%) $3.9{\cdot}10^{10}$	(18%) $9.1{\cdot}10^{10}$	(6%) $1.9{\cdot}10^{11}$	12
N	(18%) $1.7{\cdot}10^{10}$	(3%) $1.3{\cdot}10^{10}$	(2%) $7.7{\cdot}10^{9}$	(1%) $3.9{\cdot}10^{10}$	2.2
O	(9%) $8.7{\cdot}10^{9}$	(3%) $1.0{\cdot}10^{10}$	(1%) $6.4{\cdot}10^{9}$	(0%) $2.3{\cdot}10^{10}$	3.5
Ar	(0%) $3.2{\cdot}10^{8}$	(7%) $2.6{\cdot}10^{10}$	(0%) $3.2{\cdot}10^{8}$	(0%) $0.0{\cdot}10^{0}$	-

Table A.5: LEAR vacuum atomic densities in four ring sections (September 1997).

shows that the relative abundance of atoms other than hydrogen is larger in the low vacuum sections. This seems to indicate, as we also see that the pressure changes around the ring are mainly caused by changes in Hydrogen and to some extent Carbon (really CH_4) that our pressure changes are mainly due to contamination by CH_4 and H_2.

In chapter 2 we discuss briefly single Coulomb scattering of beam particles on the rest gas nuclei. In the calculation emerges a dependence on the charge of the rest gas nuclei, and one defines an 'effective' density, or single Coulomb scattering density n_{sc} (eqn. (2.2)). It is interesting to know how much the variations in rest gas composition observed in the tables above will influence this density if the same pressure is assumed. In Table A.6 n_{sc} has been calculated for the various compositions and the results are compared to the smallest obtained density.

A similar calculation can be done for the loss rate due to charge exchange with the rest gas. The result of calculating the loss rate given by equation (2.4) for the various compositions are given in Table A.7. In the calculations the measured total cross sections given in Table 2.1 have been used, including compensation for the energy difference between the cross section

Mark	Composition	n_{sc} [m^{-3}]	n_{sc}/n_{sc}^{min}
a	Table A.4, Sect.4.	$1.63{\cdot}10^{12}$	1.0
b	Table A.4, Sect.3.	$6.27{\cdot}10^{12}$	3.8
c	Table A.4, Sect.2.	$9.97{\cdot}10^{12}$	6.1
d	Table A.4, Sect.1.	$1.03{\cdot}10^{13}$	6.3
e	Table A.2, Multi, S4	$3.11{\cdot}10^{12}$	1.9
f	Table A.2, Multi, S2	$1.95{\cdot}10^{12}$	1.2
g	Table A.2, Single, S4	$3.96{\cdot}10^{12}$	2.4
h	Table A.2, Single, S2	$3.86{\cdot}10^{12}$	2.4

Table A.6: Single Coulomb scattering densities n_{sc} for the different observed vacuum compositions in LEAR calculated for a constant total pressure of $5{\cdot}10^{-12}$ Torr ($7{\cdot}10^{-10}$ Pa).

measurements and the LEAR experiments. The scaling with energy has been deduced from the empirical formula for electron capture cross sections, and we find an increase in the cross section from 4.66 MeV/amu to 4.2 MeV/amu of 27% - this has been included. For C and O we have made the linear approximation that $\sigma_{tot}^{O,C} = \sigma_{tot}^{N} Z_{O,C}/Z_N$, which according to Figure 2.1 should be reasonable.

Composition	Γ_{c-ex} [10^{-2} s^{-1}]	$\Gamma_{c-ex}/\Gamma_{c-ex}^{min}$
Table A.4, Sect.4.	0.55	1.0
Table A.4, Sect.3.	2.38	4.3
Table A.4, Sect.2.	1.79	3.3
Table A.4, Sect.1.	3.63	6.6
Table A.2, Multi, S4	1.11	2.0
Table A.2, Multi, S2	0.70	1.3
Table A.2, Single, S4	1.48	2.7
Table A.2, Single, S2	1.43	2.6

Table A.7: Charge-exchange loss rates Γ_{c-ex} for the different observed vacuum compositions in LEAR calculated for a constant total pressure of $5{\cdot}10^{-12}$ Torr ($7{\cdot}10^{-10}$ Pa).

Appendix B

Physical Properties of Matter

This appendix contains some tables of properties of matter which may be of interest in the discussions in this report.

B.1 Ionization potentials of atoms and molecules

Several aspects of the beam interactions with the vacuum and the vacuum vessels may depend on the ionization potentials of the various constituents of the vacuum and species adsorbed on the vacuum vessel. The follow Table lists a selection of ionization potentials for neutral atoms and molecules as well as singly ionized atoms (in which case it is more electron loss than ionization, but the convention seems to be that it is also referred to as ionization).

Species	Mass [amu]	Neutral E_i^0 [eV]	Singly Ionized E_i^1 [eV]	Species	Mass [amu]	Neutral E_i^0 [eV]
H	1	13.6		H_2	2	15.4
He	4	24.6	54.4	CH_4	16	12.6
C	12	11.3	24.4	H_2O	18	12.6
N	14	14.5	29.6	N_2	28	15.6
O	16	13.6	35.1	CO	28	14.0
Ne	20	21.6	41.0	O_2	32	12.1
Ar	40	15.8	27.6	CO_2	44	13.8

Table B.1: Ionization potentials of some atoms and molecules commonly found in vacuum systems [43].

B.2 Adsorption of molecules and atoms

The energy with which a molecule or atom is bound to a given surface may have a large influence on the desorption yield [61] and is therefore of interest in connection with the studies carried out

in this note. Table B.2 shows the chemisorption energies of some molecules on some different surfaces.

Species	Surface	E_{chem} [eV]	Species	Surface	E_{chem} [eV]
CO	Ni(111)	1.26	CO	Ni	1.8
CO	Cu(111)	0.52	CO	Ti	6.8
CO	Pb(111)	1.47	O	Ti	7.7
CO	Ag(111)	0.28	O	Ni	5.0
CO	Pt(111)	1.50	O	Cu	4.5
CO	Al(111)	0.21	O	Pt	4.0

Table B.2: Chemisorption energy E_{chem} of some different molecules chemisorbed on various surfaces. The measurements on the left are from 1996 [34], whereas the right ones are from 1965 - the discrepancy between the C0 on Ni result gives an impression of the uncertainty of the old method [61, 15].

The chemisorption energies in table B.2 corresponds reasonably with the statement in Ref. [58], that these energies are typically above 1 eV. The tables above and below should be considered as examples of the types of measurements which exist. Many more measurements do exist, but it is beyond the scope of this note to make a complete compilation, as it is not evident to what extent the detailed variation of binding energies, which are anyway much smaller than the kinetic energy of the lost Pb ions, influence the desorption. However, we could add that the adsorption energy of water (H_2O) on Pt(111) is 0.67 eV [24].

Table B.3 shows the physisorption energies of some molecules on glass and Carbon.

	Physisorbed Gas		
Material	H_2	N_2	O_2
Glass	0.085	0.185	0.177
Carbon	0.810	0.160	

Table B.3: Physisorption energies (in eV) for some gases on Glass and Carbon [58].

References

[1] K. Akaishi, K. Ezaki, O. Motojima and M. Nakasuga, *Production of ultra high vacuum by helium glow discharge in an unbaked vacuum chamber*, Vacuum **48**, 767 (1997)

[2] K. Akaishi, K. Ezaki, Y. Kubota, and O. Motojima, *Reduction of water outgassing and UHV production in an unbaked vacuum chamber by neon gas discharge*, Vacuum **53**, 285 (1999)

[3] *ALICE - Technical Proposal*, CERN Report, CERN/LHCC 95-71

[4] L.H. Andersen, P. Hvelplund, H. Knudsen, S. P. Møller, K. Elsener, K.-G. Rensfelt and E. Uggerhøj, *Single and Double Ionization of Helium by Fast Antiproton and Proton Impact*, Phys. Rev. Lett. **57**, 2147 (1986)

[5] J.C. Barnard, I. Bojko and N. Hilleret, *Desorption of H_2 and CO_2 from Cu by 5 keV Ar^+ and H_2^+ ion bombardment*, Vacuum **47**, no.4, 347 (1996)

[6] O. Becker, W. Knippelberg and K. Wien, *Emission of Non-Metallic Ions from a Metal Surface under Heavy-Ion Bombardment*, Phys. Script. **T6**, 117 (1983)

[7] I. Ben-Itzhak, T.J. Gray, J.C. Legg and J.H. McGuire, *Inclusive and Exclusive Cross Sections for Multiple Ionization by Fast, Highly Charged Ions in the Independent-Electron Approximation*, Phys. Rev. A **37**, 3685 (1988)

[8] C. Benvenuti, G. Canil, P. Chiggiato, P. Collin, R. Cosso, J. Guérin, S. Ilie, D. Latorre, and K. S. Neil, *Surface cleaning efficiency measurements fro UHV applications*, Vacuum **53**, 317 (1999)

[9] H. Berg, J. Ullrich, E. Bernstein, M. Unverzagt, L. Spielberger, J. Euler, D. Schardt, O. Jaqutzki, H. Schmidt-Böcking, R. Mann, P.H. Mokler, S. Hagmann and P.D. Fainstein, *Absolute Cross Sections for Helium Single and Double Ionization in Collisions with Fast, Highly Charged Projectiles*, J. Phys. B **25**, 3655 (1992)

[10] C. Bernardini, G.F. Corazza, G. Di Giugno, G. Ghigo, J. Hassinski, P. Marin, R. Querzoli, and B. Touschek, *Lifetime and beam size in a storage ring*, Phys. Rev. Lett. **10**, 407 (1963)

[11] Y. Le Beyec, *Ion Desorption Phenomena Induced by various types of Multiply Charged Projectiles and by Photons on Solid Surfaces*, ELAF91, Publ. in: Collision processes of ion, positron, electron and photon beams with matter : Eds. A. C. A. Souza *et al* (World Sci., Singapore), 31 (1991)

[12] I. Bitensky, E. Parilis, S. Della-Negra, and Y. Le Beyec, *Emission of hydrogen ions under multiply charged ion bombardment*, Nucl. Inst. & Meth. B **72**, 380 (1992)

[13] M. Blaskiewicz, L. Ahrens and H. Calvani, *Anomalous, intensity dependent losses in $Au32+$ beams*, Proc. 1997 Particle Accelerator Conference (PAC97), (Vancouver, Canada), 959 (1997)

[14] J. Bosser, C. Carli, M. Chanel, C. Hill, A. Lombardi, R. Maccaferri, S. Maury, D. Möhl, G. Molinari, S. Rossi, E. Tanke, G. Tranquille and M. Vretenar, *Experimental Investigation of Electron Cooling and Stacking of Lead Ions in a Low Energy Accumulation Ring*, Internal note, CERN/PS 99-033 (DI), (1999)

[15] D.O. Hayward and B.M.W. Trapnell, Phil. Trans. Roy. Soc. (London) A **258**, 347 (1965)

[16] R.S. Calder, *Ion induced gas desorption problems in the ISR*, Vacuum **24**, 437 (1974)

[17] K.H. Chung, S.K. Lee, Y.H. Shin, J.Y. Lim, S.S. Hong, S.H. Be, *The outgassing from TiN and BN films grown on stainless steel by IBAD*, Vacuum **53**, 303 (1999)

[18] I. R. Collins, O. Gröbner, O. B. Malyshev, A. Rossi, P. Strubin, and R. Veness, *Vacuum Stability for Ion Induced Gas Desorption*, LHC Project Report 312, CERN (1999)

[19] S. Datz, *Interactions of Multiply Charged Ions With Solids*, Physica Scripta **T3**, 79 (1983)

[20] S. Della-Negra, Y. Le Beyec, B. Monart, K. Standing, and K. Wien, *Some aspects of MeV Heavy Ion Induced Desorption from Solid Insulating Surfaces*, Nucl. Inst. & Meth B **32**, 360 (1988)

[21] O. Ellegaard, J. Schou, B. Stenum, H. Sørensen, R. Pedrys, B. Warczak, D.J. Oostra, A. Haring, and A. E de Vries, *Sputtering of solid nitrogen and oxygen by keV hydrogen ions*, Surface Science **302**, 371 (1994)

[22] R. Erlandsson, *Ion Induced Desorption from Stainless Steel studied with Isotope Techniques*, Internal note, CERN/IS/VA 80-08 (1980)

[23] E. Fischer and K. Zankel, *The Stability of the Residual Gas Density in the ISR in presence of High Intensity Proton Beams*, Internal Note, CERN/ISR/VA 73-52 (1973)

[24] G. B. Fisher and J. L. Gland, *The interaction of water with the Pt(111) surface*, Surface Science **94**, 446 (1980)

[25] B. Franzke, *Vacuum Requirements for Heavy Ion Synchrotrons*, IEEE Transactions on Nuclear Science **NS-28**, no.3, 2116 (1981)

[26] B. Franzke, *Interaction of Stored Ion Beams with the Residual Gas*, in CERN Accelerator School, CERN Yellow reports, 92-01, 100 (1992)

[27] J. K. Fremerey, *Residual gas: traditional understanding and new experimental results*, Vacuum **53**, 197 (1999)

[28] H.J. Frischkorn, and K.O. Groeneveld, *Heavy Ion Induced Electron Emission from Solid Surfaces*, Phys. Script. **T6**, 89 (1983)

[29] B. Garke, C. Edelmann, and M. Ehrt, *The influence of a glow discharge treatment on surface modification and outgassing rate of stainless steel and titanium alloys*, Vacuum **47**, no.4., 383 (1996)

[30] G.H. Gillespie, *Impact Ionzation Scaling Cross Sections for Fast Highly Stripped Ions Colliding with H_2 and He*, Phys. Lett. A **93**, 327 (1983)

[31] W. G. Graham, K. H. Berkner, R. V. Pyle, A. S. Schlachter, J.W. Stearns and J. A. Tanis, *Charge-transfer cross sections for multiply charged ions colliding with gaseous targets at energies from 310 keV/amu to 8.5 MeV/amu*, Phys. Rev. A **30**, 722 (1984)

[32] O. Gröbner and R. S. Calder, *Beam Induced Gas Desorption in the CERN Intersecting Storage Rings*, 1973 Particel Accelerator Conference, San Francisco, Publ: IEEE Transactions on Nuclear Science (USA) **20**, no.3., 760 (1973)

[33] O. Gröbner, *Dynamic Outgassing*, in "Vacuum Technology", CERN Accelerator School, ed. S. Turner (CERN 99-05, Geneva, 1999), p. 127

[34] B. Hammer, Y. Morikawa, and J. K. Nørskov, *CO Chemisorption at Metal Surfaces and Overlayers*, Phys. Rev. Lett. **76**, 2141 (1996)

[35] N. Hilleret and R. Calder, *Ion Desorption of Condensed Gases*, Internal Note, CERN-ISR-VA/77-33 (1977)

[36] S. Ichimura, K. Kokubun, M. Hirata, S. Tsukahara, K. Saito, and Y. Ikeda, *Measurement of outgassing characteristics from a vacuum chamber fabricated for pressure calibration in UHV/XHV region*, Vacuum **53**, 291 (1999)

[37] Y. Ishikawa, T. Yoshimura, and M. Arai, *Effect of surface oxide layers on deuterium permeation through stainless steels with reference to outgassing reduction in ultra- to extremely high vacuum*, Vacuum **47**, no.4.,357 (1996)

[38] J.D. Jackson, *Classical Electrodynamics*, (Second Edition, Wiley, New York), (1975)

[39] *Design study of a facility for experiments with low energy antiprotons (LEAR)*, G. Plass Eds., Internal note, CERN/PS/DL 80-7 (1980)

[40] P. Lefèvre and D. Möhl, *A Low Energy Accumulation Ring of Ions for LHC (A Feasibility Study)*, Internal Note, CERN/PS 93-62 (DI) (1993)

[41] C. Lemell, HP. Winter, and F. Aumayr, *Charge state effects in the interaction of multiply charged ions with surfaces*, Nucl. Inst. & Meth. B **125**, 146 (1997)

[42] *The Large Hadron Collider, Conceptual Design*, CERN Report, CERN/AC/95-05 (LHC)

[43] *Handbook of Chemestry and Physics*, eds. D. R. Lide, (72nd edition, CRC Press), 10-213 (1991)

[44] N. Madsen, *Dynamics of Laser-Cooled Ion Beams*, Ph.D. Thesis, Univesity of Aarhus (1998)

[45] N. Madsen, *Beam Evolution in the Antiproton Decelerator (AD) under the influence of Residual Gas and Intra Beam Scattering*, Internal Note, CERN PS/DI/Note 99-06, AD Note 047 (1999)

[46] A. G. Mathewson, *The surface cleanliness of 316 L + N stainless steel studied by SIMS and AES*, Vacuum **24**, 505 (1974)

[47] A. G. Mathewson, *Ion Induced Desorption Coefficients for Titanium Alloy, Pure Aluminium and Stainless Steel*, Internal note, CERN/ISR/VA 76-5 (1976)

[48] J.H. McGuire, A. Müller, B. Schuch, W. Groh and E. Salzborn, *Ionization of helium by highly charged ions at 1.4 MeV/amu*, Phys. Rev. A **35**, 2479 (1987)

[49] M. Minato and Y. Itoh, *Vacuum characteristics of titanium*, J. Vac. Sci. Tech. A **13**, 540 (1995)

[50] Y. Nagaim, Y. Saito and N. Matuda, *Hydrogen desorption from copper during ion bombardment measured by SIMS*, Vacuum **47**, 737 (1996)

[51] A. Poncet, *Ion trapping, clearing, beam-ion interactions*, in "Vacuum Technology", CERN Accelerator School, ed. S. Turner (CERN 99-05, Geneva, 1999), p. 127

[52] F.F. Rieke and W. Prepejchal, *Ionization Cross Sections of Gaseous Atoms and Molecules for High-Energy Electrons and Positrons*, Phys. Rev. A **6**, 1507 (1972)

[53] A.S. Schlachter, K. H. Berkner, W. G. Graham, R.V. Pyle, P.J. Schneider, K. R. Stalder, J.W. Stearns, J.A. Tanis and R.E. Olson, *Ionization of rare-gas targets by collisions of fast highly charged projectiles*, Phys. Rev. A **23**, 2331 (1981)

[54] A.S. Schlachter, K. H. Berkner, W. G. Graham, R. V. Pyle, J. W. Stearns and J.A. Tanis, *Collisions of fast, highly stripped carbon, niobium, and lead ions with molecular hydrogen*, Phys. Rev. A **24**, 1110 (1981)

[55] A. S. Schlachter, K.H. Berkner, H.F. Beyer, W. G. Graham, W. Groh, R. Mann, A. Müller, R.E. Olson, R.V. Pyle, J. W. Stearns and J.A. Tanis, *Collisions of Fast Highly Charged Ions in Gas Targets: Ionization, Recoil-Ion Production, and Charge Transfer*, Physica Scripta **T3**, 153 (1983)

[56] A.S. Schlachter, J.W. Stearns, W.G. Graham, K.H. Berkner, R.V. Pyle and J.A. Tanis, *Electron capture for fast highly charged ions in gas targets: An empirical scaling rule*, Phys. Rev. A **27**, 3372 (1983)

[57] A.S. Schlachter, K. H. Berkner, J.W. Stearns, W.G. Graham, E.M. Bernstein, M.W. Clark, J.A. Tanis, H. Schmidt-Böcking, S. Kelbch, J. Ullrich, S. Hagmann, P. Richard, M.P. Stockli and A. Müller, *Ionization and Charge Transfer in High-Energy Ion-Atom Collisions*, Nucl. Inst. & Meth. B **24/25**, 219 (1987)

[58] J.L. Segovia, *Physics of outgassing*, in "Vacuum Technology", CERN Accelerator School, ed. S. Turner (CERN 99-05, Geneva, 1999), p. 99

[59] E.F. da Silveira and M. Matos, *A pre-impact model fro ionic and atomic desorption induced by fast multicharged projectiles*, Surface Science **326**, 370 (1995)

[60] H. Straub, H. Bethe, J. Ashkin, N.F. Ramsey and K.T. Bainbridge, *Experimental nuclear physics*, Vol.1., Eds. E. Segre, (Wiley, New York), 251 (1953)

[61] E. Taglauer, W. Heiland, and U. Beitat, *The influence of adsorption energies on ion impact desorption of surface layers*, Surf. Scien. **89**, 710 (1979)

[62] O. Uwira, A. Müller, J. Linkemann, T. Bartsch, C. Brandau, M. Schmitt, W. Wolf, D. Schwalm, R. Schuch, W. Zong, H. Lebius, W. G. Graham, J. Doerfert and D.W. Savin, *Recombination measurements at low energies with* $Au^{49+,50+,51+}$ *at the TSR*, Hyperfine Interactions **108**, 149 (1997)

[63] S.Y. Zhang and L.A. Ahrens, *Booster Gold Beam Injection Efficiency and Beam Loss*, Sixth European Particle Accelerator Conference (EPAC 98), (Stockholm, Sweden), 2149 (1998)

[64] S.Y. Zhang and L.A. Ahrens, *Gold Beam Losses at the AGS Booster Injection*, Proc. 1999 Particle Accelerator Conference, (New York, USA), 3294 (1999)